Fortified LEWICE with Viscous Effects

Tuncer Cebeci,* H. H. Chen,† and N. Alemdaroğlu‡
California State University, Long Beach, California 90840

A method for computing the prediction of ice shapes on airfoils and their effects on the airfoil lift and drag coefficients are described. The previously developed LEWICE code has been modified to avoid problems due to multiple stagnation points. The interactive boundary-layer method developed by Cebeci has been incorporated into LEWICE to improve the accuracy of predicting ice shapes as well as to compute the performance characteristics of iced airfoils. The paper also presents ice shapes calculated without and with viscous effects, the consequences for aerodynamic properties, particularly lift and drag, and evaluation of the time steps used in the ice accretion process.

Nomenclature

A = damping-length constant
C_d = drag coefficient
C_l = lift coefficient
C_p = pressure coefficient
c = chord length
c_{ij} = coefficients of the Hilbert integral
k_s = equivalent sand-grain roughness
L = mixing length
R_c = chord Reynolds number, $= u_\infty c/\nu$
t = time
u,v = streamwise and normal velocity components, respectively
u_e = boundary-layer edge velocity
u_τ = friction velocity, $\equiv (\tau_w/\rho)^{1/2}$
v_n = blowing velocity
x,y = Cartesian coordinates
α = angle of attack
δu_e = perturbation velocity due to viscous effects
δ^* = displacement thickness
ν = kinematic viscosity

I. Introduction

THE problem of ice accretion on lifting bodies has been known for many years, and various solutions have been adopted including mechanical systems for removing the ice and heat transfer to prevent its formation. At the same time, research has been undertaken to improve understanding of the formation of the ice, its accretion, and the consequences for aerodynamic performance. Knowledge of this type has been assembled within numerical calculation methods such as that developed with support from the NASA Lewis Research Center and called LEWICE.[1]

It is now generally understood that the nature of the ice depends on meteorological properties so that glaze ice is formed at temperatures slightly below freezing and rime ice is increasingly superimposed as the temperature falls. Glaze ice is characterized by its buildup to large dimensions, as, for example, in the familiar horns, and rime ice by its opaque appearance with a fine-grained surface. The shape of the ice changes with time and is influenced by the nature of water droplets and ice particles that impinge on the body or are carried past it depending on their size and the flow properties, which, in turn, depend on the shape of the body. The resulting impingement, coalescence, and accretion depend on the temperatures of the surface, discrete and continuous phases, and convective heat transfer, which is again linked to the shape of the body and the nature of the flow around it. It is evident, therefore, that a mathematical description of the phenomenon of ice and its consequences for lift and drag requires the solution of time-dependent equations, albeit with comparatively low frequencies, with consideration of conservation of mass, momentum, and thermal energy for discrete and continuous phases, with a model to represent the coalescence and consideration of conduction heat transfer within the ice and possibly within the body. Some of these features are represented by the LEWICE method but with scope for improvement.

Two aspects of a calculation method are addressed in this paper, and both can be viewed within the framework of LEWICE, which combines three main features, as shown in Fig. 1. The first is concerned with the complex shape of the ice and its representation in the flowfield prediction, and the second is concerned with the incorporation of viscous effects so that lift and drag can be calculated without and with ice for a practically relevant range of angles of attack. They are, inevitably, mutually dependent and are concerned with the flowfield prediction item of Fig. 1.

In the LEWICE procedure, the calculation of the flowfield around the airfoil can be achieved in several ways. One is to solve the inviscid flow equations by a panel method, as in Ref. 1. A second is to incorporate the viscous effects by an iterative inviscid/boundary-layer method. A third is to solve the Navier-Stokes equations. All three alternatives require that the surface be free of the discontinuities that are known to exist and to influence the flowfield. The irregular ice shape, see, for example, Fig. 2, can lead to multiple stagnation points with subsequent numerical difficulties, including a breakdown of the trajectory calculations that are necessary to determine the spatial distribution of water droplets.

A plausible way to overcome the difficulties caused by multiple stagnation points is to introduce a smoothing proce-

Fig. 1 Structure of LEWICE.

Received Oct. 27, 1989; presented as Paper 90-0754 at the AIAA 28th Aerospace Sciences Meeting, Reno, NV, Jan. 8-11, 1990; revision received May 1, 1990; accepted for publication Sept. 1, 1990.
Copyright © 1990 by the American Institute of Aeronautics and Astronautics, Inc. All rights reserved.

*Professor and Chairman, Aerospace Engineering Department. Fellow AIAA.
†Associate Professor, Aerospace Engineering Department. Member AIAA.
‡Lecturer, Aerospace Engineering Department. Member AIAA.

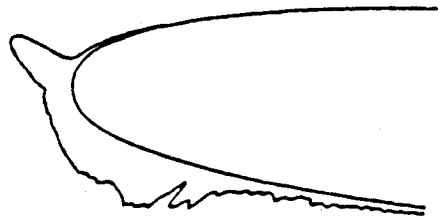

Fig. 2 Example of real ice accretion from Ref. 3.

dure that reduces the amplitude of the surface irregularities without loss of important flow characteristics. The LEWICE[1] employs a smoothing technique that requires operator control, with consequent arbitrariness and inconvenience. In addition, this approach does not allow consistent consideration of the ice buildup for more than 2 min. A consequence of this method is that the flowfield calculation corresponds to a time different from that of the ice geometry and, since the process is nonlinear, errors of unknown magnitude can result. Thus, it is desirable to automate the process of surface smoothing in a manner that does not remove features with important consequences for the flow. The calculation method must then be able to represent flows with multiple stagnation points and do so efficiently so that results can be obtained as the ice changes shape with time.

Much of the available information on the effect of ice on aerodynamic properties comes from a series of experiments, which includes those of Gray and von Glahn,[4] Bragg and Gregorek,[5,6] Bragg et al.,[7] Korkan et al.,[8] Bragg,[9] Bragg and Coirier,[10] Korkan et al.,[11] and Bragg and Spring.[12] It includes consideration of several airfoils and results in terms of lift and drag coefficients and the nature of separation bubbles. In particular, Bragg and Coirier[10] simulated a glaze ice accretion on a 21-in. chord model NACA 0012 airfoil and reported measurements of surface pressures, lift, and drag coefficients. Detailed velocity profiles indicated the large regions of reversed flow caused by the ice and the corresponding substantial increase in drag and reduction in lift. The stall angle, which without ice was around 16 deg, was reduced to 6 deg.

These experiments confirm the need to represent viscous effects for accurate calculations of all aerodynamic properties, and this has consequences for the cost of the results, particularly since the problem is time dependent. It should be noted that the viscous effects can be incorporated into the flowfield calculations and into the ice accretion process so that the droplet trajectories and the heat transfer coefficient, which is flowfield dependent, can be calculated more accurately. The results of Fig. 3 confirm the importance of the viscous effects in the leading-edge region of an iced airfoil, but the consequences for ice formation are unknown.

The viscous effects may be incorporated by solving the Navier-Stokes equations or by use of interaction between solutions of inviscid and boundary-layer equations. We prefer the second approach, particularly since, with the added complication of time dependence, the need of economy is important. The methodology has been proven for clean and iced airfoils, for example, by Cebeci et al.[13] and Cebeci,[14] and shown to be much more economical to implement than solutions of higher order forms.[15]

In light of the preceding comments, this paper has been prepared to describe and test procedures in order to avoid problems with multiple stagnation points, to allow incorporation of viscous effects, and to examine the consequences of the nonlinear nature of ice accretion. The tests involve comparison of ice shapes achieved without and with viscous effects, the consequences for aerodynamic properties, particularly lift and drag, and evaluation of the extent of the nonlinearity.

The following section describes the essential features of the present inviscid-viscous interaction method. The third section begins with a description of the procedure used to deal with

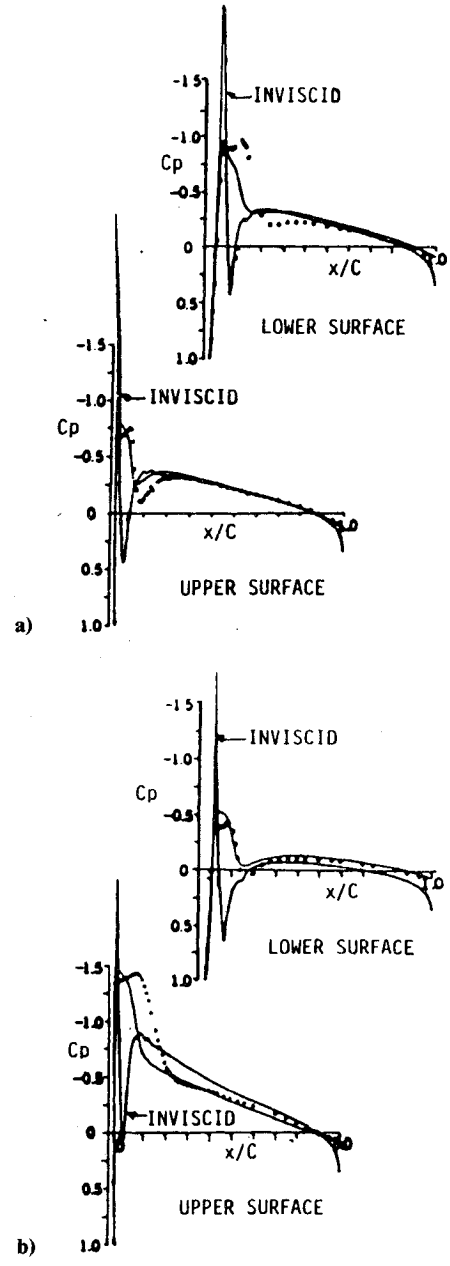

Fig. 3 Comparison of measured (symbols) and computed (solid lines, inviscid and viscous) pressure coefficients corresponding to the iced NACA 0012 airfoil of Ref. 12 at two angles of attack: a) $\alpha = 0$ deg; b) $\alpha = 4$ deg. (The figure is from Ref. 14.)

multiple stagnation points and presents results based on the flow over a NACA 0012 airfoil at several angles of attack without and with viscous effects. The results include ice shapes, pressure distributions, and lift and drag coefficients. A summary of the more important conclusions is given in Sec. IV. Reference 16 describes the changes to the input and output routines of the computer program previously reported in Ref. 1.

II. Inviscid-Viscous Interaction Method

The interactive boundary-layer method described by Cebeci[14] provides the foundation to include the viscous effects in the LEWICE code. It comprises solution procedures for inviscid-flow and boundary-layer equations and a procedure that couples them together so as to ensure that each influences the other. The inviscid-flow equations are solved by a form of the panel method devised by Hess and Smith,[17] the boundary-layer solution procedure is based on Keller's box scheme, and the finite-difference approximations are written for conservation equations expressed in terms of Falkner-Skan variables.

The eddy-viscosity formulation[18] is used in regions of transitional and turbulent flow, and the onset of turbulence is specified by the expression of Ref. 19 or by the occurrence of laminar separation. These features of the method are outlined in Sec. II-A, with a more complete description of the procedures used to deal with the nonaerodynamic nature of ice accretions in Sec. II-B.

A. Interactive Boundary-Layer Method

Studies with conformal mapping and panel methods showed that the latter were more suitable for the geometrical arrangements of ice, and the present panel method defines the airfoil and ice by a set of points in the physical plane. Neighboring points are connected by straight-line panels that each have source density and vorticity. The vorticity strength of each panel is the same so that vorticity is defined by a total strength, adjusted to satisfy the Kutta condition. The source strengths have different values on each panel that are adjusted, by solving a set of simultaneous linear equations, to satisfy the normal-velocity boundary condition at the midpoints of the panels. In the strictly inviscid case, this condition requires that the total normal velocity, freestream plus body sources and vortices, should vanish. When the boundary layer is simulated, the desired normal velocity v_n is finite and equals the derivative along the surface of the product of tangential velocity and displacement thickness $\mathrm{d}/\mathrm{d}s\ (u_e\delta^*)$. It is known that this surface blowing distribution displaces the dividing streamline outward from the surface of the airfoil to the location of the displacement thickness. Experience has shown that best results are obtained when surface pressures are calculated and the Kutta condition is applied on the displacement surface rather than on the surface panels.

The boundary-layer equations for two-dimensional external steady incompressible flows are well known and are solved here with the external velocity distribution obtained from inviscid flow theory. With $u_e^o(x)$ denoting the inviscid velocity distribution and $\delta u_e(x)$ the perturbation velocity due to viscous effects,

$$u_e(x) = u_e^o(x) + \delta u_e(x) \tag{1}$$

$$\delta u_e(x) = \frac{1}{\pi}\int_{x_a}^{x_b} \frac{\mathrm{d}}{\mathrm{d}\sigma}(u_e\delta^*)\,\frac{\mathrm{d}\sigma}{x-\sigma} \tag{2a}$$

where $\mathrm{d}(u_e\delta^*)/\mathrm{d}\sigma$ is the blowing velocity, and the interaction is confined to the range $x_a \le x \le x_b$.

In this form, Eq. (2a) provides an outer boundary condition for the viscous-flow calculations that represent the viscous-inviscid interaction and can be generalized to the form

$$u_e(x) = u_e^\kappa(x) + \sum_{j=1}^{n} c_{ij}[(u_e\delta^*)_j - (u_e\delta^*)_j^\kappa] \tag{2b}$$

where $u_e^\kappa(x)$ corresponds to the inviscid velocity distribution that contains the displacement thickness effect $(\delta^*)^\kappa$ computed from a previous sweep. Here, c_{ij} denotes the interaction-coefficient matrix, which is obtained from a discrete approximation to the Hilbert integral.

The numerical solution of the boundary-layer equations, written in transformed variables, is obtained with the box method for both standard (given pressure distribution) and interactive methods. This second-order finite-difference method has been used extensively by Cebeci and his associates for a wide range of flows.[20] As in previous studies, an inverse form of the equations is used to obtain the solutions with separation and, as before, the FLARE approximation, in which the convective term $u(\partial u/\partial x)$ is set equal to zero in the recirculating region, is employed. No attempt was made to improve the accuracy of the solutions resulting from this approximation. The nonlinear system of algebraic equations that results from the finite-difference approximations is linearized by Newton's method and solved by a block elimination procedure. It should be noted that the mixing-length expression of the Cebeci-Smith model[18] has been modified to deal with surface roughness such as that associated with ice: the modification is to the mixing length with the wall-damping expression,

$$L = \kappa(y + \Delta y)\{1 - \exp[-(y + \Delta y)/A]\} \tag{3}$$

where Δy is a function of an equivalent sand-grain roughness k_s. In terms of dimensionless quantities, with $k_s^+ = k_s u_\tau/\nu$ and $\Delta y^+ = \Delta y u_\tau/\nu$,

$$\Delta y^+ = \begin{cases} 0.9[\sqrt{k_s^+} - k_s^+ \exp(-k_s^+/6)] & 5 < k_s^+ \le 70 \\ 0.7(k_s^+)^{0.58} & 70 \le k_s^+ \le 2000 \end{cases} \tag{4}$$

In order to convert the roughness into equivalent sand-grain roughness, the procedure of Smith and Kaups[21] is used with the ratio of the equivalent sand-grain roughness to the roughness of the applied elements k_s/k, assumed to be a function of the concentration and shape of the roughness elements.

B. Procedures to Deal with Leading-Edge Ice Shapes

Ice on airfoils can introduce substantial geometric changes to their leading edges in a short period and can cause rapid variations in the flow properties. As a result, the inviscid and viscous-flow calculations may have difficulty in producing satisfactory solutions. For the boundary-layer calculations, the iced airfoil is regarded as a smooth or rough surface obtained by covering the leading-edge region with a "blanket," as shown in Fig. 4. It also makes use of a continuation method in that the initial calculations are performed for the smooth airfoil and subsequent ones for a series of shapes that fall between the smooth and iced airfoils. For each shape, the blowing velocity is computed from

$$v_n = \frac{\mathrm{d}}{\mathrm{d}x}[u_e(\delta^* - \delta)] \tag{5}$$

where δ^* corresponds to the displacement thickness obtained from the boundary-layer solutions for the shape whose geometrical difference from the smooth airfoil is $\delta^{(i)}(x)$ and where the δ^* surface is outside the singularity surface. This allows the viscous effects to be incorporated into the inviscid-flow solutions gradually, at each time step, thus reducing the sensitivity of the viscous-flow solutions to the rapid changes in the pressure distribution near the leading edge. For further details, see Ref. 14.

III. Results and Discussion

The flowfield calculations in the fortified LEWICE code have the option of computing the flowfield without and with viscous effects. In the present study, we used both options to examine the effect of viscosity on the formation of the ice shape. Of course, in both options, the code computes the lift and drag characteristics of the airfoil.

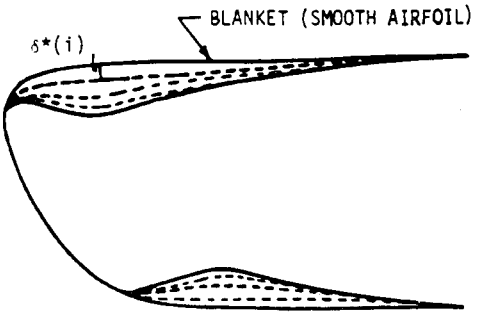

Fig. 4 Boundary-layer model used in the viscous-flow calculations.

In either option, it is necessary to devise an operator-free procedure to avoid the occurrence of the multiple stagnation points caused by the formation of irregular surfaces such as horns and feathers on the ice shape. In the present study, we used a smoothing procedure that checks the ice shape and replaces the region with multiple stagnation points with a pseudosurface, as described in the following.

For a given pressure distribution with more than one stagnation point, we assume that the flowfield requires modifications and we use a subroutine called PSURF to form a pseudosurface over the zone with multiple calculated stagnation points. Since they are caused by the existence of a dent on the surface, the subroutine checks to see whether there is any concave surface over the region of multiple stagnation points. If there is, then a pseudosurface, which is a cubic polynomial curve based on Hermite or osculatory interpolation,[22] is used. According to this procedure, the surface is defined by specifying the two endpoints and their slopes, as discussed in Ref. 22. The two endpoints on the curve are the locations where the pseudosurface intersects the actual ice. With the use of a Hermite polynomial, the ends of the pseudosurface curve intersect on a tangent to the ice surface. This is a very appropriate smoothing procedure because the added pseudosurface approximates the actual ice surface as close to its original shape as possible.

After the pseudosurface is placed over the troubled area, the flowfield calculation is repeated. In general, the calculated pressure distribution is much smoother than that of the actual ice shape in the stagnation region and has only one stagnation point so that the calculations can be continued for times much longer than those previously accomplished with LEWICE, which used an operator-controlled smoothing procedure.

The fortified LEWICE code has been used to calculate the ice shapes on a NACA 0012 airfoil for a range of angles of attack without and with viscous effects for glaze and rime ice on a 0.30-m chord airfoil for the following conditions for glaze ice: freestream velocity = 129.46 m/s; freestream temperature = 260.55 K (or -12.45°C); freestream pressure = 90,748 Pa; liquid water content = 0.50 g/m^3; droplet diameter = 20.0 μm; and relative humidity = 100%. The icing conditions for a rime ice are the same as those for the glaze ice except that the freestream velocity is 64.73 m/s.

Section III-A presents the results for an inviscid ice in which the flowfield calculations do not have viscous effects in them. There are two main changes in the present code. The first is that it uses a more efficient panel method and performs the trajectory calculations more efficiently with approximately 65% less computer time for a 2-min ice. Our calculations indicate that the computer time of the present code for a 5-min ice is equivalent to that of LEWICE for a 2-min ice. The second difference is the smoothing procedure, which is now operator free.

Section III-B presents the results for a viscous ice in which the flowfield calculations contain the viscous effects. Again, the calculations are performed for a range of angles of attack. In these cases, however, the range of angle of attack is limited because, with increase in ice shape or angle of attack, the maximum lift coefficient of the iced airfoil is significantly different from that of a clean airfoil.

With the inclusion of viscous effects in the flowfield calculations, we have also conducted parametric studies to show the effect of roughness on the formation of ice shape and lift and drag. With the turbulence model that accounts for roughness, we performed calculations for two values of equivalent sand-grain roughness k_s. The first, $k_s/c = 0.001$, corresponds to the carborundum grains used on the rough airfoils discussed in Ref. 14, and the second, $k_s/c = 0.002$, provides a value higher than that likely to be experienced.

In Sec. III-C, we present results that examine the nonlinear nature of the ice accretion process. Rather than determine ice shape corresponding to the pressure distribution at a previous time, we introduce an intermediate time so as to reduce the lag between pressure distribution and ice shape. In addition, we performed calculations to determine the effect of time steps on the ice shapes.

A. Inviscid Ice

The ice shapes of Fig. 5 correspond to angles of attack of 0, 4, and 8 deg and to times up to 10 min with time steps Δt of 1 min. At $\alpha = 0$ deg, the results retain symmetry and were performed for 5 min without any signs of numerical difficulty. It can be seen that the horns are rugged so that modifications would be required to extend the results. At $\alpha = 4$ deg, the results extend to 10 min with a shape that becomes increasingly asymmetric and smoother with increasing time. These characteristics are also evident at $\alpha = 8$ deg, where the results extend to 14 min. The expected buildup of ice on the downstream region of the pressure surface should be noted. For convenience of comparison, Fig. 6 shows the ice shapes after 3 min for angles of attack of 0, 4, and 8 deg. It is interesting to note that at $\alpha = 0$ deg the forward extent of the 3-min ice buildup is around 3% chord, whereas at $\alpha = 8$ deg it exceeds 5% chord. Its downstream extent at $\alpha = 8$ deg is considerable with measurable thickness beyond 50% chord.

Figure 7 shows the results for a rime ice at zero incidence for times up to 10 min with time steps Δt of 1 min. As in the case of glazed ice, the results retain symmetry at small times but begin to display slight asymmetry at larger times. The calculations show no numerical difficulties in computing the ice shape.

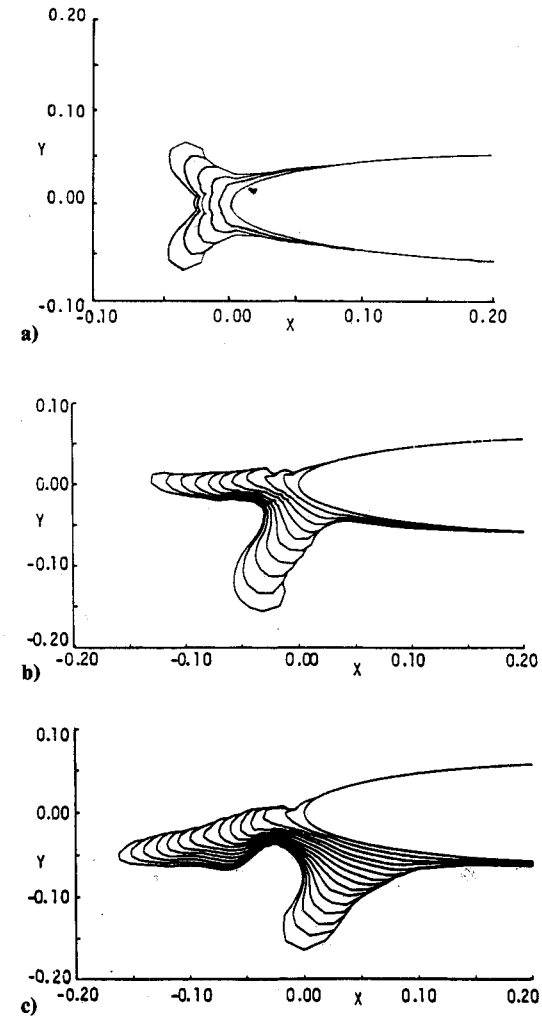

Fig. 5 Computed inviscid glazed ice shapes at three angles of attack: a) $\alpha = 0$ deg; b) $\alpha = 4$ deg; c) $\alpha = 8$ deg.

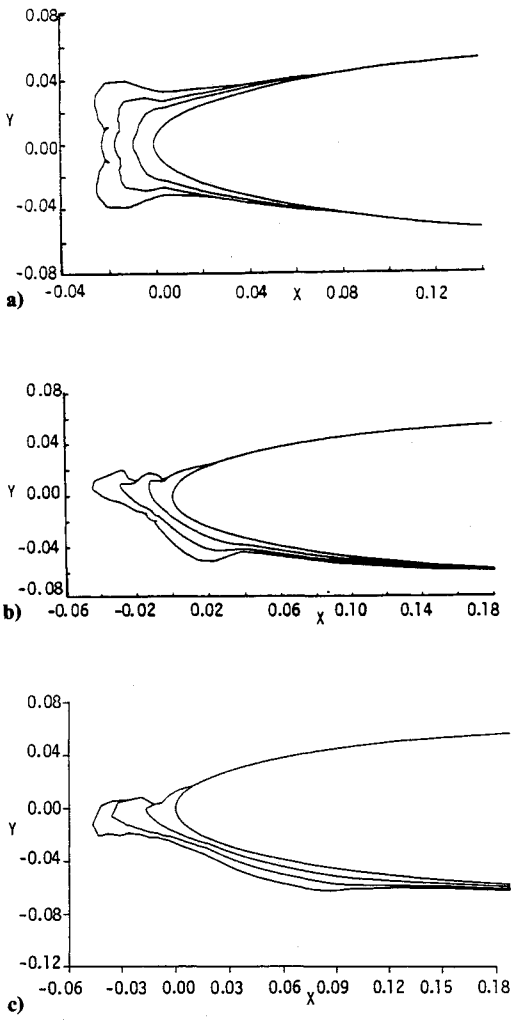

Fig. 6 Computed inviscid glazed ice shapes at three angles of attack for 3 min: a) $\alpha = 0$ deg; b) $\alpha = 4$ deg; c) $\alpha = 8$ deg.

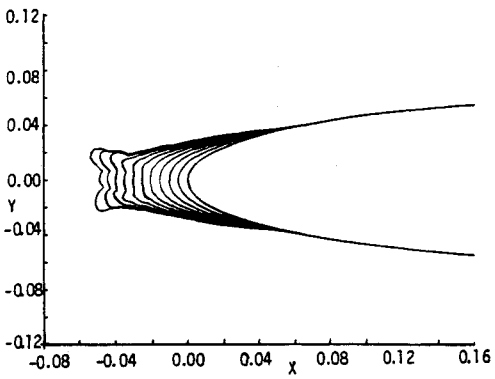

Fig. 7 Computed inviscid rime ice at $\alpha = 0$ deg.

B. Viscous Ice

The glaze viscous ice results of Fig. 8 show that the total ice accretion is the same with and without viscosity for $\alpha = 0$ deg. At two higher angles of Fig. 8, the viscous ice differs from the inviscid ice with time. The effects are relatively small at small times but become bigger with increasing time. With the incorporation of viscosity, it became more difficult to calculate for large times so that the results of Fig. 8 do not extend beyond 4 min. Again, modifications to the present automatic procedure can lead to results for longer times, though limitations must exist as discussed later.

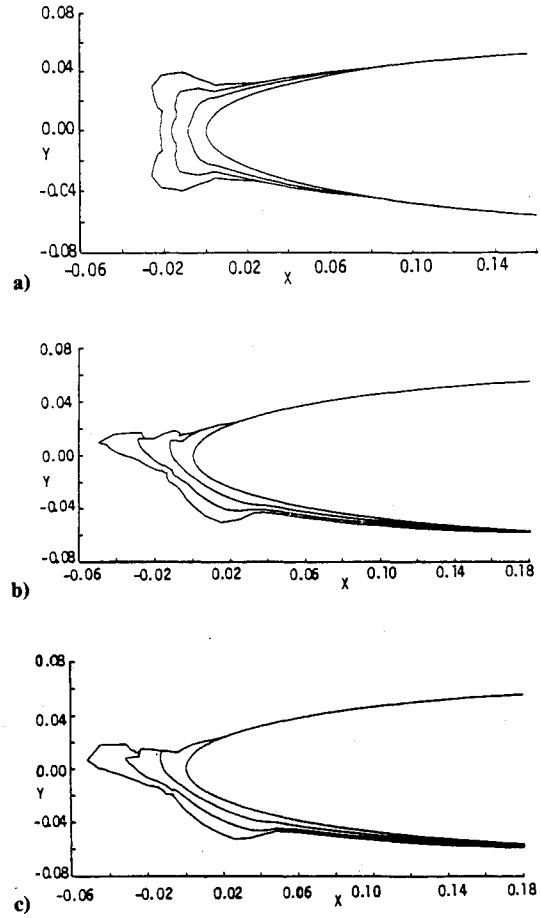

Fig. 8 Computed viscous glazed ice shapes at three angles of attack without roughness: a) $\alpha = 0$ deg; b) $\alpha = 4$ deg; c) $\alpha = 5$ deg.

Pressure distributions with all shapes referred to previously and those of Fig. 9, corresponding to $\alpha = 4$ deg, are typical. The figure shows the progression of the pressure coefficient distributions with time. With ice buildup, the pressure distribution computed by the panel method and the boundary-layer method are essentially the same except around the leading edge. The ice accretions cause rapid changes in the pressure distribution with leading-edge peaks that are very large, as might be expected from the results of Fig. 8. Without the viscosity effects, these peaks were even larger, as indicated in Fig. 3, and are not reproduced here. Even with the reductions in pressure peaks associated with viscous effects, local separation is very likely with the result that the envelope of flow separation region will reduce the peak as in Fig. 3. Here, we have devised a procedure where the leading-edge peaks are averaged to provide a smooth pressure distribution, again similar to those measured and shown in Fig. 3. As time increases, the ice builds up, the suction surface maximum is reduced, and, with it, the toal lift is reduced; since the effect is confined to the first 10% of chord, the reduction is small, as we shall discuss shortly.

Table 1 shows drag coefficients for viscous ice with and without surface roughness for $\alpha = 0$ deg. In this case, the lift is practically zero in all cases. The drag coefficient, on the other hand, increases substantially with time and particularly over the first time interval. The effect of roughness is comparatively small but increases with time so that, for example, 20% of the drag coefficient is associated with roughness for 3-min ice. We were unable to obtain results for 4-min ice with roughness. At $\alpha = 4$ deg, Table 2 shows that the viscous lift coefficient increases slightly with time in harmony with the inviscid lift. The reduction in lift due to viscosity is $< 5\%$ and is nearly independent of time and, therefore, ice shape. The effect of roughness on lift is small but, even for zero angle of

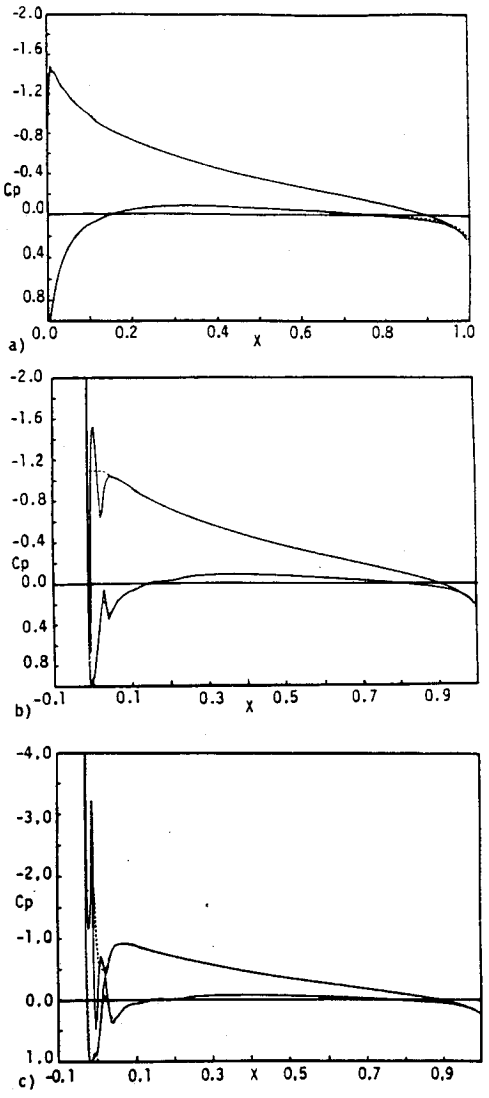

Fig. 9 Pressure distributions for $\alpha = 4$ deg. Dashed and solid lines denote viscous and inviscid values: a) $t = 0$ min; b) $t = 1$ min; c) $t = 2$ min.

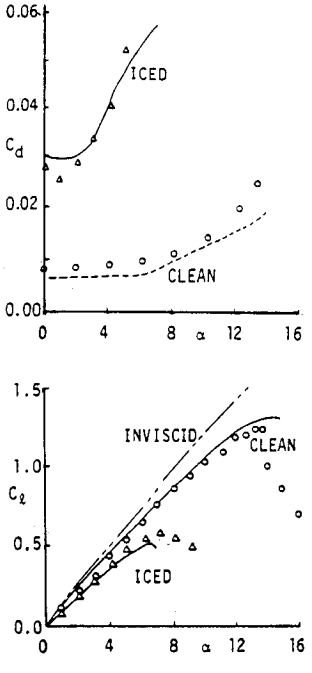

Fig. 10 Computed lift and drag coefficients for the NACA 0012 iced and clean airfoil. Symbols denote the data of Ref. 12.

attack, the drag coefficient increases substantially with time, and roughness plays a greater role in that it adds 30–50% to the drag coefficient for 2-min ice.

It should be noted that the similarity between the lift coefficients with and without ice at 4-deg angle of attack is characteristic of angles from 0 to 4 deg, as shown in Fig. 10, reproduced from Ref. 14. The experimental data of this show the substantial reduction in maximum lift coefficient with ice and that the effects are comparatively small up to around $\alpha = 5$ deg. It can also be seen that the calculation method represents the increasing divergence of the experimental data from the inviscid results. The drag coefficients of Fig. 10 show a large increase with angle of attack of around 4 deg and that the calculation method is accurate up to around $C_{l\max}$.

Figure 11 shows that the buildup of rime ice for zero angle of attack is more orderly than that of glaze ice. The calculations were performed for times up to 5 min and could readily have been extended. As before, the effect of ice on the lift coefficient was negligible and the drag coefficient, as shown in Table 3, increased more than 30% for 1-min ice and was, thereafter, constant. The effect of roughness is small.

C. Nonlinear Ice Accretion

In the calculations presented in the preceding sections, the flowfield used in the ice formation corresponded to a previous time. Since the calculations were performed with time steps of 1 min starting from a clean airfoil, the computed ice shape at 1 min made use of the pressure distribution on the clean airfoil, which is substantially different from that at 1 min. In the study of the effect of this assumption, we performed calculations with a range of time steps.

Figure 12 shows the results for $\alpha = 4$ deg obtained with a lag of half that of Fig. 6b by using the following procedure: a

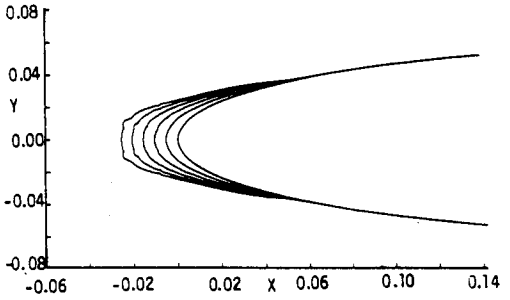

Fig. 11 Computed viscous rime ice shape at $\alpha = 0$ deg.

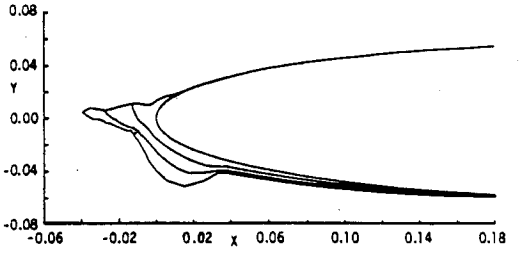

Fig. 12 Computed nonlinear inviscid ice shapes for $\alpha = 4$ deg.

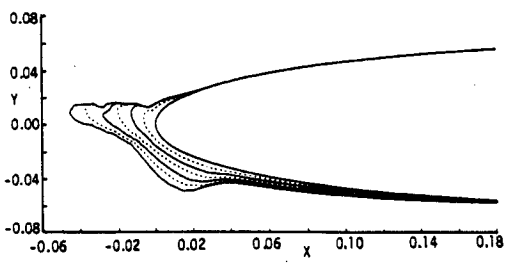

Fig. 13 Computed inviscid ice shapes for $\alpha = 4$ deg, $\Delta t = 0.5$ min.

Table 1 Drag coefficients for glaze ice, $\alpha = 0$ deg and $R_c = 2.9 \times 10^6$

t	Without roughness	Roughness, $k_s/c = 0.001$	Roughness, $k_s/c = 0.002$
0	0.00674	—	—
1	0.00980	0.0105	0.0108
2	0.00989	0.0108	0.0111
3	0.0101	0.0118	0.0123
4	0.0103	—	—

Table 2 Lift and drag coefficients for glaze ice, $\alpha = 4$ deg and $R_c = 2.9 \times 10^6$

t	Without roughness	Roughness, $k_s/c = 0.001$	Roughness, $k_s/c = 0.002$
	Lift coefficient		
0	0.446	—	—
1	0.448	0.442	0.443
2	0.451	0.433	0.427
	Drag coefficient		
0	0.00744	—	—
1	0.0103	0.0129	0.0140
2	0.0106	0.0134	0.0152

Table 3 Drag coefficients for rime ice, $\alpha = 0$ deg and $R_c = 1.5 \times 10^6$

t	Without roughness	Roughness, $k_s/c = 0.001$	Roughness, $k_s/c = 0.002$
0	0.00729	—	—
1	0.0109	0.0114	0.0117
2	0.0110	0.0114	0.0117
3	0.0110	0.0114	0.0117
4	0.0110	—	0.0118
5	0.0110	—	0.0117

pressure distribution (PD) was first calculated for a clean airfoil, then another PD for an ice shape obtained with $\Delta t = 1$ min. A new 1-min ice shape was then calculated for the PD obtained by averaging the two PDs computed previously. This procedure was then repeated for other ice shapes at $t = 2$ and 3 min. In this case, it is clear that the two results differ by amounts that are likely to be important. The reduction in the lag results in less ice accretion, particularly at higher times and from the greatest forward protrusion.

Figure 13 shows the results for $\alpha = 4$ deg obtained with a time interval half of Fig. 6b, that is, $\Delta t = 0.5$ min. The effect is clearly less than that associated with the nonlinear effects, and the result shows little difference from that of Fig. 6b, obtained with $\Delta t = 1$ min.

IV. Concluding Statements

The methodology of the LEWICE computer program has been improved to allow hands-off calculation of ice shapes without the problems associated with multiple stagnation points. The results of computer times have been reduced around 65%. The effects of viscosity have been included through an interactive boundary-layer procedure and the numerical method arranged to consider the nonlinear ice accretion process. Testing of this fortified LEWICE code has shown that it will calculate inviscid ice accretion up to 14 min for angles of attack of around 9 deg and viscous ice accretion for shorter times.

The results for ice accretion show that viscous effects increase with time and angle of attack but are comparatively small. The effects of roughness are also small but nonlinear aspects appear to be more important.

Calculations of lift and drag coefficients have been performed and the former shows that, at lower angles of attack, the reduction in the lift coefficient of iced airfoils is similar to that associated with the inclusion of viscous effects. It is known, however, that the iced airfoil will stall at an angle of attack considerably less than that of a clean airfoil. Consideration of viscous effects is essential to the determination of drag, and the results show that ice increases the drag coefficient by some 35% at angles of attack up to 4 deg. The drag coefficients increase further in excess of 20% with roughness effects which depend on the sand-grain roughness parameter and angle of attack.

The present results indicate that the effects of ice can be important to lift and drag but are necessarily limited in their scope. It is essential that the calculations be performed for a range of airfoil shapes and angles of attack up to stall. These calculations should involve ice accretions for longer times than those considered here. Also, the consequences for ice on slat/airfoil configurations should be determined. The fortified LEWICE code provides the basis for these extensions but further improvements are necessary. In particular, the hands-off smoothing procedure must be improved to allow calculation of ice accretion to extend to longer times at low angles of attack. In addition, the effects of nonlinearity and step lengths need further investigation and the incorporation of a preferred arrangement. At the same time, further work should be directed to the improvement of the ice accretion model. It should be noted that the methodology described here can be extended to deal with icing on three-dimensional configurations including wings and engine intakes. Three-dimensional inviscid- and viscous-flow methods exist and can be tailored to these problems.

Acknowledgment

This work was supported by the NASA Lewis Research Center under Grant NAG 3-935.

References

[1]Ruff, G. A., "User's Manual for the NASA Lewis Ice Accretion Prediction Code (LEWICE)," NASA Rept., 1986.

[2]Shaw, R. J., Potapczuk, M. C., and Bidwell, C. S., "Predictions of Airfoil Aerodynamic Performance Degradation Due to Ice," *Numerical and Physical Aspects of Aerodynamic Flows, IV*, edited by T. Cebeci, Springer-Verlag, New York, 1989.

[3]Gent, R. W., Markiewicz, R. H., and Cansdale, J. T., "Further Studies of Helicopter Rotor Ice Accretion and Protection," *Proceedings of the 11th European Rotorcraft Forum,* 1985.

[4]Gray, V. H., and von Glahn, U. H., "Aerodynamic Effects Caused by Icing of an Unswept NACA 65A004 Airfoil," NACA TN-4155, 1957.

[5]Bragg, M. B., and Gregorek, G. M., "Wind Tunnel Investigation of Airfoil Performance Degradation due to Icing," AIAA Paper 82-0582, March 1982.

[6]Bragg, M. B., and Gregorek, G. M., "Predicting Aircraft Performance Degradation Due to Ice Accretion," Society of Automotive Engineers, Warrendale, PA, Paper 83074, April 1983.

[7]Bragg, M. B., Zaguli, R. J., and Gregorek, G. M., "Wind Tunnel Evaluation of Airfoil Performance Using Simulated Ice Shapes," NASA CR-167960, Nov. 1982.

[8]Korkan, K. D., Dadone, L., and Shaw, R. J., "Performance Degradation of Helicopter Rotor Systems in Forward Flight due to Rime Ice Accretion," AIAA Paper 83-0029, Jan. 1983.

[9]Bragg, M. B., "Predicting Airfoil Performance with Rime and Glaze Ice Accretions," AIAA Paper 84-0106, Jan. 1984.

[10]Bragg, M. B., and Coirier, W. J., "Detailed Measurements of the Flowfield in the Vicinity of an Airfoil with Glaze Ice," AIAA Paper 85-0409, Jan. 1985.

[11]Korkan, K. D., Cross, E. J., and Cornell, C. C., "Experimental Aerodynamic Characteristics of an NACA 0012 Airfoil with Simulated Ice," *Journal of Aircraft,* Vol. 22, No. 2, 1985, pp. 130–134.

[12]Bragg, M. B., and Spring, S. A., "An Experimental Study of the Flowfield About an Airfoil with Glaze Ice," AIAA Paper 87-0100, Jan. 1987.

[13]Cebeci, T., Clark, R. W., Chang, K. C., Halsey, N. D., and Lee, K., "Airfoils with Separation and the Resulting Wakes," *Journal of Fluid Mechanics,* Vol. 163, 1986, p. 323.

[14]Cebeci, T., "Calculation of Flow Over Iced Airfoils," *AIAA*

Journal, Vol. 27, No. 7, 1989, pp. 853-861.
[15]Chang, K. C., Alemdaroğlu, N., Mehta, U., and Cebeci, T., "Further Comparisons of Interactive Boundary-Layer and Thin-Layer Navier-Stokes Procedures," *Journal of Aircraft,* Vol. 25, No. 10, 1988, pp. 897-903.
[16]Cebeci, T., Chen, H. H., and Alemdaroğlu, N., "Fortified LEWICE with Viscous Effects," NASA CR (in print).
[17]Hess, J. L., and Smith, A. M. O., "Calculation of Potential Flow About Arbitrary Bodies," *Progress in Aeronautical Sciences,* Vol. 8, edited by Kuchemann, 1964.
[18]Cebeci, T., and Smith, A. M. O., *Analysis of Turbulent Boundary Layers,* Academic, New York, 1974.
[19]Michel, R., "Etude de la Transition sur les Profiles d'Aile; Establissement d'un Critere de Determination de Point de Transition et Calcul de la Trainée de Profile Incompressible," Office National d'Etudes et de Recherches Aérospatiales, Rept. 1/1578A, 1951.
[20]Bradshaw, P., Cebeci, T., and Whitelaw, J. H., *Engineering Calculation Methods for Turbulent Flows,* Academic, London, England, 1981.
[21]Smith, A. M. O., and Kaups, K., "Aerodynamics of Surface Roughness and Imperfections," Society of Automotive Engineers, Warrendale, PA, Paper 680198, April 1968.
[22]Cebeci, T., and Bradshaw, P., *Physical and Computational Aspects of Convective Heat Transfer,* Springer-Verlag, New York, 1989.

Recommended Reading from the AIAA Progress in Astronautics and Aeronautics Series . . . AIAA

Dynamics of Explosions and Dynamics of Reactive Systems, I and II

J. R. Bowen, J. C. Leyer, and R. I. Soloukhin, editors

Companion volumes, *Dynamics of Explosions and Dynamics of Reactive Systems, I and II*, cover new findings in the gasdynamics of flows associated with exothermic processing—the essential feature of detonation waves—and other, associated phenomena.
Dynamics of Explosions (volume 106) primarily concerns the interrelationship between the rate processes of energy deposition in a compressible medium and the concurrent nonsteady flow as it typically occurs in explosion phenomena. *Dynamics of Reactive Systems* (Volume 105, parts I and II) spans a broader area, encompassing the processes coupling the dynamics of fluid flow and molecular transformations in reactive media, occurring in any combustion system. The two volumes, in addition to embracing the usual topics of explosions, detonations, shock phenomena, and reactive flow, treat gasdynamic aspects of nonsteady flow in combustion, and the effects of turbulence and diagnostic techniques used to study combustion phenomena.

Dynamics of Explosions
1986 664 pp. illus., Hardback
ISBN 0-930403-15-0
AIAA Members $54.95
Nonmembers $92.95
Order Number V-106

Dynamics of Reactive Systems I and II
1986 900 pp. (2 vols.), illus. Hardback
ISBN 0-930403-14-2
AIAA Members $86.95
Nonmembers $135.00
Order Number V-105

***TO ORDER:* Write, Phone or FAX:** AIAA c/o TASCO,
9 Jay Gould Ct., P.O. Box 753, Waldorf, MD 20604
Phone (301) 645-5643, Dept. 415 • FAX (301) 843-0159

Sales Tax: CA residents, 7%; DC, 6%. Add $4.75 for shipping and handling of 1 to 4 books (Call for rates on higher quantities). Orders under $50.00 must be prepaid. Foreign orders must be prepaid. Please allow 4 weeks for delivery. Prices are subject to change without notice. Returns will be accepted within 15 days.